State-dependent olfactory processing in freely behaving mice

Mary R. Schreck[1,*], **Liujing Zhuang**[1], **Emma Janke**[1], **Andrew H. Moberly**[1], **Janardhan P. Bhattarai**[1], **Jay A. Gottfried**[2], **Daniel W. Wesson**[3], **Minghong Ma**[1,4,*]

[1]Department of Neuroscience, University of Pennsylvania Perelman School of Medicine, Philadelphia, PA 19104, USA

[2]Department of Psychology, University of Pennsylvania, School of Arts and Sciences; Department of Neurology, University of Pennsylvania Perelman School of Medicine, Philadelphia, PA 19104, USA

[3]Department of Pharmacology and Therapeutics, University of Florida, Gainesville, FL 32610, USA

[4]Lead contact

SUMMARY

Decreased responsiveness to sensory stimuli during sleep is presumably mediated via thalamic gating. Without an obligatory thalamic relay in the olfactory system, the anterior piriform cortex (APC) is suggested to be a gate in anesthetized states. However, olfactory processing in natural sleep states remains undetermined. Here, we simultaneously record local field potentials (LFPs) in hierarchical olfactory regions (olfactory bulb [OB], APC, and orbitofrontal cortex) while optogenetically activating olfactory sensory neurons, ensuring consistent peripheral inputs across states in behaving mice. Surprisingly, evoked LFPs in sleep states (both non-rapid eye movement [NREM] and rapid eye movement [REM]) are larger and contain greater gamma-band power and cross-region coherence (compared to wakefulness) throughout the olfactory pathway, suggesting the lack of a central gate. Single-unit recordings from the OB and APC reveal a higher percentage of responsive neurons during sleep with a higher incidence of suppressed firing. Additionally, nasal breathing is slower and shallower during sleep, suggesting a partial peripheral gating mechanism.

Graphical Abstract

*Correspondence: mschreck@pennmedicine.upenn.edu (M.R.S.), minghong@pennmedicine.upenn.edu (M.M.).

In brief

Schreck et al. examine how the olfactory system responds to the same peripheral stimulus during natural sleep and wake in mice. Larger responses along the pathway during sleep suggest the lack of a central gate, but slower and shallower breathing may act as a partial peripheral gate to reduce olfactory input.

INTRODUCTION

One of the hallmarks of sleep is decreased responsiveness to sensory stimuli. This phenomenon is referred to as state-dependent sensory gating, and for most sensory systems, sleep/wake-dependent gating involves the thalamus. The emergence of delta oscillations (0.5–4 Hz) and thalamic spindles (8–14 Hz) during non-rapid eye movement (NREM) sleep are thought to curtail sensory information flow, thus minimizing alertness, arousal, and active neural processes (McCormick et al., 2015). While sleep-induced response attenuation has been widely observed in the primary visual, somatosensory, and auditory cortices (Brugge and Merzenich, 1973; Gucer, 1979; Livingstone and Hubel, 1981; Murata and Kameda, 1963; Sharon and Nir, 2018), more recent work in the auditory system challenges this prevailing view of the "thalamic gate," given that sound-evoked responses are in fact preserved in auditory cortex during sleep (Issa and Wang, 2008, 2011; Nir et al., 2015; Sela et al., 2016).

By comparison, the olfactory system is a distinct exception to the rule: information can reach olfactory cortical areas without an obligatory thalamic relay (Courtiol and Wilson, 2016; Mori and Sakano, 2021). Odor information originates with the binding of odorants to specific receptors expressed on the olfactory sensory neurons (OSNs) in the nose, which project to a few discrete glomeruli in the olfactory bulb (OB). OB projection neurons carry information to the olfactory cortices, including the anterior piriform cortex (APC), which then transmits information to the orbitofrontal cortex (OFC), either directly or indirectly through the mediodorsal (MD) nucleus of the thalamus (Courtiol and Wilson, 2016; Mori and Sakano, 2011; Price and Slotnick, 1983; Yarita et al., 1980). Indeed, it follows that the olfactory system might be impervious to thalamic gating, or at least relies on different state-dependent processing during sleep. To this point, humans typically do not waken in response to an odor during sleep, but there is ample evidence for olfactory processing during sleep (Arzi et al., 2010; Badia et al., 1990; Carskadon and Herz, 2004; Stuck et al., 2006, 2007). If a background odor is presented while subjects take part in an object-location memory task, delivery of this same odor during sleep will activate relevant fMRI categorical representations and enhance subsequent post-sleep memory performance (Rasch et al., 2007; Shanahan et al., 2018). Likewise, during aversive conditioning between a visual stimulus and mild electric shock, an accompanying contextual odor will induce behavioral extinction if that odor is delivered in sleep (Hauner et al., 2013). Modulation of olfactory fear memories during sleep has also been observed in rodents (Barnes and Wilson, 2014; Rolls et al., 2013). Finally, learning to associate a tone with a pleasant odor can be achieved during sleep, eliciting deeper breaths in response to the tone, despite subjects' having no recollection of the odor (Arzi et al., 2012). Together, these studies bring compelling evidence that the olfactory pathway is functionally active during sleep.

Some of the strongest support for state-dependent gating in the olfactory system comes from data in anesthetized rodents, suggesting a gate in the APC (Murakami et al., 2005; Wilson, 2010). Single-unit recordings in the APC of anesthetized rats uncovered reduced responses to odorants in the slow-wave (sleep-like) state, while responses in the OB are comparable between slow-wave and fast-wave (wake-like) states (Murakami et al., 2005; Wilson, 2010). In local field potential (LFP) recordings of anesthetized rats, coherence between the OB and the piriform cortex decreases in the slow-wave state, while it is strengthened between higher cortical regions, suggesting the OB is offline from the olfactory cortex during sleep (Wilson and Yan, 2010). In naturally sleeping rats, gamma oscillations in response to an odorant are dampened during NREM sleep in the APC (Barnes et al., 2011). However, interpretation of these studies is challenging, either due to the use of anesthesia, which can substantially modify sensory responses compared with awake animals (Fontanini and Bower, 2005; Kato et al., 2012; Kollo et al., 2014; Rinberg et al., 2006; Vincis et al., 2012; Wachowiak et al., 2013), or due to altered peripheral inputs, namely, changes in odor inhalation and odor sampling, as breathing rate and amplitude are lower during sleep (Friedman et al., 2004; Jessberger et al., 2016).

It remains undetermined whether the olfactory system processes information differently in natural sleep versus wake states. Here we addressed this question in freely behaving mice using multi-site electrophysiology combined with optogenetics to overcome the previous technical challenges. Optogenetic activation of OSNs, while not recapitulating physiological

input of a given odor, ensured that peripheral inputs remained consistent within the same animal across different states, while LFPs were simultaneously recorded from hierarchical olfactory areas (OB, APC, OFC, and/or MD) or single-unit recordings were obtained from the OB or APC. Surprisingly, OSN stimulation-evoked responses were larger or stronger in nearly all parameters measured (LFP amplitude, area under the curve, root-mean-square amplitude, gamma oscillation power, cross-region coherence) in all recorded sites in sleep than in wakefulness. Single-unit recordings from both the OB and the APC revealed similar numbers of neurons displaying increased firing upon OSN stimulation in both wake and sleep, but more neurons showed suppressed firing during sleep than during wake. Suppressed firing among these neurons during sleep may make stimulus-evoked excitatory responses in other neurons more prominent by reducing the background noise. Furthermore, analysis of nasal breathing confirmed slower respiration rates and shallower inhalation slopes during sleep. Overall, our findings argue against a central olfactory gate, and instead support a reduction in peripheral odor input during sleep.

RESULTS

OSN stimulation evokes larger LFPs along the olfactory pathway in sleep states than in wakefulness

To study how the olfactory system transmits information under different brain states, we used electrophysiology coupled with optogenetics in freely behaving mice. Mice were implanted with bipolar electrodes in multiple areas along the olfactory pathway (OB, APC, and OFC) and were recorded from for 3 to 4 h/day. The electromyogram (EMG) from the neck muscle and LFPs from either the APC or the OFC were used *post hoc* to determine the sleep/wake state (Figure S1A). Wake was characterized by low-amplitude, fast LFP oscillations and high EMG activity. NREM sleep was characterized by high-amplitude, low-frequency LFP oscillations in the delta range (0.5–4 Hz) and low EMG activity, whereas REM sleep was defined by LFP oscillations in the theta range (6–8 Hz) and even further reduced EMG activity (Figure S1B).

To ensure consistent peripheral inputs across sleep/wake states, an optical fiber was implanted in the nasal cavity of OMP-ChR2 mice, in which OSNs express channelrhodopsin 2 (ChR2) under the control of the olfactory marker protein (OMP) gene. Blue laser stimulation, consisting of five 5–150 ms pulses at 0.5 Hz, was delivered approximately once every 5 min to yield OSN input to the OB while minimizing potential response adaptation. In most experiments, the pulse width of 150 ms was chosen to mimic the length of the inhalation cycle when the mouse breathes at approximately 3 Hz, which occurs during sleep (Friedman et al., 2004; Jessberger et al., 2016). LFPs were simultaneously recorded from the OB, APC, and OFC (Figures 1A and S1C). Each laser pulse evoked a transient change in the LFP (Figures 1B and 1C), which was extracted and quantified from peak to trough as the LFP amplitude. In a subset of mice, shorter pulse durations (5 and 50 ms) were also tested, and the evoked LFPs in the OB and APC showed a state dependence similar to those evoked by 150 ms pulses (Figures S1D and S1E). Control OMP-Cre mice lacking ChR2 did not show light-evoked responses, indicating these were a result of OSN activation, not an optical/electrical artifact (Figure 1C).

We reasoned that if a state-dependent "gate" exists along the ascending olfactory pathway, then OSN stimulation would induce a larger response in wake than in sleep, with significant response decrement at and after the "gate." Surprisingly, we observed greater LFP amplitudes during NREM sleep than during wake along the olfactory pathway at all three recording sites (OB, APC, and OFC) (Figures 1C and 1D). This was observed in 25 of 27 mice for the OB, 16 of 17 mice for the APC, and all 19 mice for the OFC recordings (Figure 1D). To determine state-dependent differences across mice, the averaged LFP amplitude was normalized to NREM sleep in each mouse. All regions showed a significant difference, with the LFP amplitude in wakefulness being 75.9% for OB, 71.8% for APC, and 70.9% for OFC of that in NREM sleep (Figure 1E). We also compared two additional parameters of the evoked LFPs (area under the curve and root-mean-square amplitude [RMS]), which showed similar state-dependent differences compared with the LFP amplitude (Figure S1F). Indeed, there were strong positive correlations between the LFP amplitude and both area under the curve and RMS (Figure S1G), presumably due to similar waveforms of the evoked LFPs across states. Based upon this, we used the LFP amplitude for subsequent analyses. These evoked LFPs were collected from the highest laser intensity that each mouse slept through (see STAR Methods for details). Since the gating properties of a sensory system may vary depending on the stimulus intensity (Issa and Wang, 2011), we conducted similar analyses at varying laser intensities and observed the same trend, i.e., larger responses in the NREM sleep state than in wakefulness (Figures 1F and 1G).

We next tested whether the LFP amplitude was attenuated along the olfactory pathway during NREM sleep in 12 mice in which OSN stimulation-induced LFPs were recorded in all three regions (OB, APC, and OFC). The LFP amplitude ratio of (OB WAKE/APC WAKE)/(OB NREM/APC NREM) was 1.07 ± 0.05 (mean $\pm$ SEM), not significantly different from 1 (Mann-Whitney U test, $p = 0.146$). Similarly, the LFP amplitude ratio of (APC WAKE/OFC WAKE)/(APC NREM/OFC NREM) was not significantly different from 1 (0.98 ± 0.05; Mann-Whitney U test, $p = 0.146$). These results suggest that there is no state-dependent attenuation in LFP amplitude along the OB-APC-OFC pathway.

In a subset of mice, laser stimulations were also delivered during REM sleep, which occurred less frequently (Weber et al., 2015). Among all the laser stimulations across different animals, approximately 42.9% occurred during wake, 45.6% during NREM sleep, and 11.3% during REM sleep. The NREM and REM sleep states displayed similar evoked LFPs (Figures 2A and 2B). The majority of mice did not show significantly different responses between the two sleep states in the recorded regions: 16 of 21 mice for the OB, 8 of 12 mice for the APC, and 12 of 14 mice for the OFC recordings (Figure 2C). Overall, the LFP amplitude during REM sleep was 95.0%, 97.2%, and 98.2% in the OB, APC, and OFC, respectively, compared with that during NREM sleep (Figure 2D). In comparisons of all three states, the wake state was significantly different from both the NREM and the REM sleep states (Figures S2A–S2D). OSN stimulation-evoked responses in the two sleep states were very similar despite the fact that their spontaneous LFP activity was different (Figures S1A and S1B). These data indicate that the olfactory pathway transmits larger evoked LFPs during sleep.

OSN stimulation induces greater gamma-band power changes in sleep states than in wakefulness

The larger LFP amplitude could be due to increased activity among the population of neurons contributing to the LFP or from stronger synchronization across the population. To assess neural synchronization, we next analyzed LFP gamma-band oscillations (30–100 Hz). Gamma oscillations are involved in the synchronization of neuronal firing in interconnected brain regions and associated with higher cognitive functions, including sensory perception (Gray and Singer, 1989; Lepousez and Lledo, 2013; Mori et al., 2013; Singer and Gray, 1995; Stopfer et al., 1997). If state-dependent olfactory processing occurs in the form of gamma oscillations, one may expect a higher power during wake than during sleep, as previously suggested (Barnes et al., 2011; Mori et al., 2013). The power of spontaneous gamma oscillations was higher during wake than during NREM sleep in all olfactory regions monitored (Figure S3A). Optogenetic stimulation of OSNs induced gamma oscillations in all three states in OMP-ChR2 mice (Figure 3A) but not in OMP-Cre control animals (Figure S3D). The power of gamma oscillations was calculated in 150 ms time bins and averaged across trials. To average across mice, two different normalization approaches were taken. First, the gamma-band power was normalized to the pre-stimulation value (−150 ms) in each state (Figures 3B and 3C). The power of induced gamma oscillations showed a greater increase during NREM sleep than during wake (Figure 3B), at least partially due to the low pre-stimulation (i.e., spontaneous) value (Figure S3A). In the subset of mice with OSN stimulation during both sleep states, the gamma-band power was similar (Figure 3C). Second, the gamma-band power for each mouse was normalized to the pre-stimulation value (−150 ms) during NREM sleep (Figures S3B and S3C). In all three states, the gamma-band power reached similar levels during stimulation (Figures S3B and S3C).

Another aspect of synchrony is interregional coherence, which is considered important for large-scale neural coordination and communication (Bastos et al., 2015; Fries, 2015). If the APC acts as a gate, we would expect enhanced OB-APC coherence during wake compared with sleep, with enhanced APC-OFC coherence during sleep (Wilson and Yan, 2010). We first compared cross-region coherence of the three recorded sites and found a higher spontaneous coherence in the gamma band in wake than in sleep states for APC-OFC and OB-OFC (Figures S4A and S4B). We then compared cross-region coherence before (PRE), during (STIM), and after (POST) light stimulation. The change in coherence between regions was calculated by subtracting the PRE value from the STIM value (Figure 4A). Gamma-band coherence increased more during NREM sleep than during wake across all regions (Figure 4B). This increase was short lived, as there was no difference in the coherence between the PRE and the POST values (Figure 4B). The change in coherence was specific to the laser stimulation in OMP-ChR2 mice, as the control mice did not show such a change (Figures S4C and S4D). Similar to other parameters compared, the NREM and REM sleep states showed similar cross-region coherence (Figures 4C and 4D). Taken together, these findings indicate that, even during sleep, the olfactory pathway can transmit information in the form of enhanced gamma oscillations and cross-region coherence.

OSN stimulation evokes larger LFPs in the MD thalamus in sleep states than in wakefulness

While sensory information can reach the olfactory cortices in the absence of a thalamic relay, there is an indirect route from the APC to the OFC through the MD thalamus (Courtiol and Wilson, 2014; Plailly et al., 2008; Price and Slotnick, 1983; Tham et al., 2011; Yarita et al., 1980). To test whether gating occurs in the MD, we recorded light-evoked LFPs in the MD of OMP-ChR2 mice. Similar to other olfactory regions, the evoked responses were larger in both NREM and REM sleep states compared with wakefulness, with the wake LFP amplitude being 72.4% of that of NREM sleep (Figures 5 and S5). Therefore, the pattern of larger LFPs in sleep states holds even in the MD thalamus.

More OB and APC units change firing rates during NREM sleep than during wakefulness

Previous studies have suggested state-dependent changes in single-unit activity in the APC but not in the OB under anesthesia (Murakami et al., 2005; Wilson, 2010). If sleep/wake-dependent gating is reflected by the APC single-unit firing patterns, one may expect stronger firing responses during wake than during sleep in the APC, but not in the OB. To test this, we analyzed spontaneous and OSN stimulation-induced firing of OB and APC single units (Figures 6 and S6). We recorded 29 single units in the OB from 12 mice (Figures 6A–6C) and 68 single units in the APC from 11 mice (Figures 6D–6F and S6). A significantly higher percentage of OB neurons were responsive to optogenetic OSN stimulation compared with the APC neurons (OB, 20 of 29, or 69.0% versus APC, 19 of 68, or 27.9%; $\chi^2_{(n=1, n=97)}$ = 14.23, p = 1.62 × 10^{-4}), possibly due to global inhibition in the olfactory cortical circuits (see discussion). Interestingly, among the 20 responsive OB neurons, 19 (or 95.0%) responded to OSN optogenetic stimulation during NREM sleep (12 with increased and 7 with decreased firing rates), while only 11 (or 55.0%; $\chi^2_{(n=1, n=40)}$ = 8.53, p = 0.0035) responded in wakefulness (11 with increased firing rates) (Figures 6A–6C). The same trend, but to a lesser extent, was observed in the APC. Among the 19 responsive APC neurons, 13 (or 68.4%) responded during NREM sleep (5 with increased and 8 with decreased firing rates), while only 8 (or 42.1%; $\chi^2_{(n=1, n=38)}$ = 2.66, p = 0.102) responded in wakefulness (7 with increased and 1 with decreased firing rates) (Figures 6D–6F and S6). Given that LFPs mainly reflect summated synaptic currents, a higher percentage of responsive neurons is consistent with larger evoked LFPs during sleep. We next compared the overall firing rates of single units between the two states (Table S1). When all OB and APC neurons were included, there was no significant difference between states. However, when only OSN stimulation-responsive neurons were included, the average firing rate of APC single units was higher in wake than in NREM sleep, which was not observed in the OB (Table S1). Notably, more OB and APC single units showed decreased firing rates in NREM sleep than in wake, which may offset the effects from single units with increased firing rates. The implications of these findings on state-dependent information transmission are further discussed.

Peripheral inputs carried by nasal breathing differ between sleep and wakefulness

The above results show that OSN stimulation-evoked responses were generally enhanced along the olfactory pathway (from the OB to OFC) during sleep. Given that olfactory input

into the nose depends on nasal breathing, which depends upon sleep/wake state (Douglas et al., 1982; Friedman et al., 2004; Jessberger et al., 2016), we hypothesize that respiration-dependent odor sampling may act as a peripheral "gate" and contribute to state-dependent olfactory perception. Using a pressure sensor or thermocouple in the nasal cavity, we recorded nasal air pressure or flow, respectively, and analyzed multiple facets of respiration via the BreathMetrics MATLAB toolbox (Noto et al., 2018) (Figure 7A). As anticipated, compared with wakefulness, respiration in NREM sleep was slower, with an average of 2.85 Hz (cf, 5.56 Hz in wake), and smaller peak flow (both inspiratory and expiratory) (Figures 7B, 7C, and S7A). Despite the larger-amplitude respiratory signal during wake, the inhale and tidal volumes were not significantly different between states (Figures 7D and S7A). Although a similar amount of air was exchanged between the two states, airflow patterns themselves are important for peripheral odor input and perception (Mainland and Sobel, 2006; Wachowiak, 2011). We found that the slope of inhalation was significantly sharper during wake (Figure 7E), which represents faster airflow (such as in sniffs) that brings odor molecules into contact with the olfactory epithelium. Additional analysis of five mice recorded for longer periods to capture enough REM sleep bouts showed similar respiration patterns between the two sleep states, distinct from the wake state (Figures S7B–S7E). These results indicate that respiration patterns are state dependent in manners that would directly impact peripheral odor input arriving into the nasal cavity.

DISCUSSION

In this study, we have investigated how the olfactory system transmits a sensory signal in naturally occurring wake and sleep states in freely behaving mice. We demonstrated that optogenetic activation of OSNs elicits larger LFPs, including heightened gamma-band power and coherence along the ascending olfactory pathway (OB, APC, and OFC) in both NREM and REM sleep states compared with wake (Figures 1, 2, 3, and 4). Larger LFPs are also observed in the MD nucleus of the thalamus in both sleep states (Figure 5). Given that the OFC is the neocortical region critically involved in olfactory perception (Li et al., 2010), our study argues against the presence of a so-called "gate" in the central olfactory pathway that simply dampens information propagation during sleep. These results are consistent with previous reports that odor processing does occur during sleep (Arzi et al., 2012, 2014; Hauner et al., 2013).

The larger evoked LFPs during both NREM and REM sleep across a wide range of stimulation durations and intensities seem counterintuitive. It is worth noting that the larger evoked LFPs along the olfactory pathway during sleep are unlikely to be due to better preservation of low-frequency signals in a low-frequency background (e.g., spontaneous activity in the NREM sleep state) because the evoked responses during REM sleep are similar to those in NREM sleep even though the spontaneous activity in REM sleep more resembles that in the awake state (Figure S1). Mechanistically, the larger LFPs evoked by OSN stimulation during sleep could arise from multiple factors. Since the LFP primarily represents summated synaptic currents at the recording site rather than firing rates (Buzsaki et al., 2012), the higher percentage of responsive OB and APC neurons during NREM sleep may contribute to the larger LFPs observed (Figure 6). Additionally, state-dependent neuromodulation may be another contributing factor. For instance, norepinephrine has been

implicated in auditory sensory arousals (Hayat et al., 2020) and visual perceptual ability (Gelbard-Sagiv et al., 2018). Norepinephrine levels are high during wakefulness and low during both sleep states (Lee and Dan, 2012; Lorincz and Adamantidis, 2017), which show similar evoked LFPs. Another mechanism that may contribute to the larger LFPs during sleep may be related to top-down cortical inputs to the OB, which mainly excite OB inhibitory interneurons, including the granule cells. These top-down inputs are stronger during wake than during anesthesia (Boyd et al., 2012, 2015; Otazu et al., 2015), and if they are also weaker during natural sleep, they would contribute to stronger inhibition during wake. Future studies are required to dissect the contributions of these different factors.

From single-unit recordings, we found more cells responding to OSN stimulation with a higher incidence of suppressed firing during NREM sleep than during wake (Figure 6). At the population level, the overall firing rates during stimulation were not significantly different in either the OB or the APC (Table S1). Odor coding in the piriform cortex is thought to be achieved via populations of spatially distributed, sparsely activated cells (Illig and Haberly, 2003; Miura et al., 2012; Poo and Isaacson, 2009; Qiu et al., 2021; Rennaker et al., 2007; Stern et al., 2018; Stettler and Axel, 2009). The earliest OB inputs might have the most importance for coding in the piriform cortex and behavior because of the recurrent cortical circuitry (Bolding and Franks, 2018; Chong et al., 2020). Decoding analysis of piriform responses in rats performing a task suggests that the spike rate rather than latency or temporal pattern leads to better odor classification (Miura et al., 2012). When we compared only single units that significantly changed their firing rates upon OSN stimulation, the overall firing rate was reduced in the APC during NREM sleep but not in the OB (Table S1). One may argue for the existence of a gate at the APC, similar to what is seen in urethane-induced slow- versus fast-wave states (Murakami et al., 2005). However, this view oversimplifies the fact that some neurons did not respond during wake but had suppressed activity during sleep. In both the OB and the APC, there were similar numbers of units excited by OSN stimulation during sleep and wake (12 versus 11 in OB and 5 versus 7 in APC) (Figure 6). Interestingly, an additional group of cells showed suppressed firing during sleep but not wake (7 versus 0 in OB and 8 versus 1 in APC). We hypothesize that suppressed firing in these neurons during sleep may make stimulus-evoked excitatory responses in other neurons more prominent by increasing the signal-to-noise ratio. If this is the case, our finding from single-unit recordings also does not support a central olfactory gate. Knowing the specific cell types (excitatory or inhibitory) of single units recorded would help to further clarify data interpretation. There is a possibility that response quality, but not necessarily its strength, carries meaningful information (Kato et al., 2012). Although the sensory signal may be present during sleep, additional mechanisms outside the olfactory pathway (e.g., state-dependent neuromodulation or "consciousness switches") may be required to achieve sensory perception (Lee and Dan, 2012; Lorincz and Adamantidis, 2017; Redinbaugh et al., 2020; Vesuna et al., 2020).

One major way this study differs from previous studies of state-dependent olfactory processing is the use of optogenetic activation of OSNs. The main advantage of this approach is the ability to provide the same peripheral stimulus to freely behaving animals across different sleep/wake states. One potential drawback is that the optogenetic approach may not exactly mimic natural odor stimulation. While we are activating a large number of

OSNs, which may not happen naturally, it is important to note that we are not saturating the stimulus or the response, as evidenced by the intensity-response curves. In fact, similar sleep/wake differences are observed even at the lowest laser intensity or with the shortest duration (Figures 1 and S1). Emerging evidence in the field suggests that optogenetic stimulation of OSNs elicits activity similar to an odor. Similar percentages of mitral/tufted (M/T) cells respond to laser stimulation of OMP-ChR2 OSNs and to an odorant (Li et al., 2014; Smear et al., 2011). In a simple go/no-go task, OMP-ChR2 mice are able to report odor presence using laser stimulation at 90% accuracy after being trained with odors (Smear et al., 2011). Mice can even report optogenetic stimulation of a single odorant receptor (OR) subtype using M72-ChR2 mice. The presence of an M72 ligand significantly decreases task performance, suggesting that optogenetic stimulation and odorants activate the same pathway (Smear et al., 2013). Optical stimulation of an M72-ChR2 glomerulus paired with a foot shock can lead to fear learning (Bhattarai et al., 2020; Vetere et al., 2019). Mice trained using the optogenetic stimulus will avoid the M72 ligand acetophenone in a two-chamber assay even though they have never experienced it (Vetere et al., 2019). Despite some differences from odors, optogenetic stimulation of OSNs has been successfully used to probe information processing in the olfactory system.

One area in which optogenetic stimulation may differ from natural odor pertains to respiration. We did not control for where in the respiratory cycle the optogenetic stimulus occurred. Mice are able to reliably perceive brief optogenetic stimulations placed at different parts of the respiratory cycle (Li et al., 2014; Rebello et al., 2014; Smear et al., 2011, 2013). However, shifting the optogenetic stimulation of glomeruli relative to the sniff cycle has less impact on task performance than shifting the order of glomeruli stimulation relative to each other (Chong et al., 2020). In our study, for each animal, tens of trials were conducted in each state. It is very likely that the stimulations have tiled the respiratory cycle and our results cannot be explained by having all the wake trials at a similar part of the respiratory cycle and the sleep trials at a different part. In many studies, odors are presented to mice for many seconds, which would also cover multiple respiratory cycles. Another way in which the stimulus varied from natural odors is that the optogenetic stimulus was not necessarily the ideal activating stimulus for the specific single units recorded from, which may explain some differences with previous studies (Murakami et al., 2005; Wilson, 2010). Although optogenetic activation of OSNs may not exactly mirror the physiology occurring in response to an odor stimulus, our study reveals what happens in the olfactory pathway when given identical peripheral inputs in wake and sleep states.

Given that our electrophysiological measures in the central olfactory pathway revealed mostly enhanced responses during sleep compared with wake, we turned our attention to state-dependent peripheral inputs into the nasal cavity. Although the tidal volume (i.e., the amount of air exchange during inhalation and exhalation) stays consistent in sleep and wakefulness, there are important state-dependent differences in respiration patterns, including slower breathing rate and shallower inhalation slope in sleep (Figures 7 and S7). It is thought that active sensing via rapid sniffing provides some advantage to the mouse, as sniffing brings the odors into contact with the epithelium more quickly (Wachowiak, 2011; Wesson et al., 2009). Increased flow rate and active sampling are shown to modify and enhance OB responses (Courtiol et al., 2011; Jordan et al., 2018; Verhagen et al., 2007). The

idea of active sensing is not unique to the olfactory system. In the visual system, saccades act to bring the region of interest into the visual field of the fovea, and pupil constriction during sleep helps to maintain the sleep state (Yuzgec et al., 2018). In the somatosensory system, people move their fingers back and forth for touch discrimination, and mice assess the environment by whisking, changing response dynamics compared with passive exposure (Ferezou et al., 2006; Pereira et al., 2007). Although an odor may be present in both sleep and wake, how it is sampled by the periphery could significantly affect sensation and perception (Mainland and Sobel, 2006; Wachowiak, 2011). This notion together with our results leads us to propose that reduced nasal inhalation during sleep contributes to state-dependent olfactory processing as a partial peripheral "gate."

Limitations of the study

There are several specific limitations we wish to highlight. First, we chose to use optogenetics to stimulate OSNs rather than natural odors. While this approach had the advantage of precisely controlling the peripheral input independent of respiration and sleep/wake state, we cannot conclude decisively that the effects we observed will apply to natural odors. Second, we did not time our stimulation to the respiratory cycle as discussed above. Third, our optogenetic stimulation did not carry biological salience to the mouse. It did not represent a learned or innately attractive or aversive odor, which might influence responses during sleep, as reported in fruit flies (French et al., 2021). Finally, knowing specific cell types of single units recorded would help to further clarify data interpretation.

STAR★METHODS

Detailed methods are provided in the online version of this paper and include the following:

RESOURCE AVAILABILITY

Lead contact—Further information and requests for resources and reagents should be directed to and will be fulfilled by the lead contact, Minghong Ma (minghong@pennmedicine.upenn.edu).

Materials availability—This study did not generate new unique reagents.

Data and code availability

- Data reported in this paper will be shared by the lead contact upon request.

- This paper does not report original code.

- Any additional information required to reanalyze the data reported in this paper is available from the lead contact upon request.

EXPERIMENTAL MODEL AND SUBJECT DETAILS

OMP-Cre mice (the coding region of OMP was replaced by that of Cre; JAX Stock No: 006668) (Li et al., 2004) and Rosa-floxed-STOP-ChR2-EYFP mice (or Ai32 line; JAX Stock No: 024109) (Madisen et al., 2012) were crossed to obtain $OMP^{Cre/WT}RosaChR2^{(f/WT)}$ (in brief, OMP-ChR2) mice. For *in vivo* electrophysiology, 2-

to 8- month male and female OMP-ChR2 mice were used. The number of male and female mice is mentioned in each figure legend. OMP$^{Cre/WT}$ (or OMP-Cre) mice without ChR2 were used as controls. Experimental mice were single housed and recorded in their home cages. Mice were kept on a regular 12/12hr light/dark cycle (7 am to 7 pm light on) with ad libitum food and water. All procedures were approved by the University of Pennsylvania Institutional Care and Use Committee.

METHOD DETAILS

Surgical implantation—Mice were exposed to isoflurane at 3% (vol/vol oxygen) for anesthetic induction. They were then secured in a stereotaxic system (Model 940, David Kopf Instruments) and isoflurane levels were reduced to 1.5% for the remainder of the surgery. Body temperature was maintained at 37°C with a temperature control system (TC-1000, CWE). For mice with LFP implants, custom 3D pieces were designed using Tinkercad (Autodesk Inc) and printed courtesy of the University of Pennsylvania's Libraries' Biomedical Library with design consultation. Bipolar tungsten electrodes (50 μm bare diameter, PFA coated, A-M Systems) were connected via gold pins (Neuralynx Inc) to an EIB-16 board (Neuralynx Inc) or a custom printed board and thread through the holes in the 3D piece. The 3D piece allowed for easy implantation of bipolar tungsten electrodes in multiple olfactory areas: OB (+4.3 mm AP, +1.0 mm ML, 1.5 mm DV), APC (+1.1 mm AP, 2.7 mm ML, 4.3 mm DV), and OFC (+2.5 mm AP, +1.5 mm ML, 2 mm DV). In a subset of mice bipolar electrodes were also implanted in the MD (−1.5 mm AP, +0.4 mm ML, 3.0 mm DV). Two stainless steel electrodes (50 μm bare diameter, A-M Systems) were implanted in the neck muscle for EMG recordings. Bilateral screws were implanted above the cerebellum for reference and grounding wires. Implants were secured using vet bond and dental cement.

For single-unit recordings in the APC, modified microdrives (Anikeeva et al., 2011) with three NiCr (25.4 μm bare diameter, A-M Systems) tetrodes were implanted. Additionally, bipolar tungsten electrodes were implanted in the OB for LFPs and stainless steel electrodes were implanted in the neck for EMG recordings. Bilateral screws were implanted above the cerebellum for reference and grounding wires. Tetrode impedance was measured using an IMP-2AMC (Bak Electronics) and lowered with gold plating solution (Neuralynx Inc). Single-unit recordings from the OB were acquired from the bipolar tungsten wires described above.

For respiration recordings, two different approaches were used. Either a thermocouple or intranasal cannula (P1 Technologies) was implanted into the nasal cavity (Verhagen et al., 2007; Wesson et al., 2008). An 8-pin surface mount board (Pinnacle Technology, 8415-SM) was secured to the skull for EEG/EMG recording. Skull screws were implanted into the hippocampus (~ −1.5 mm AP, ~ +1.5 mm ML) and two stainless steel wires were implanted in the neck muscle. Bilateral screws were implanted above the cerebellum for reference and grounding. For intranasal canula mice, the following day a partial contralateral naris occlusion was performed using a cauterizer (Fine Science Tools) to increase the robustness of respiration recording. Mice recovered for 5–7 days following surgery before recordings were performed.

Optogenetic stimulation—In addition to the implants for recording neural signals, a 0.39 NA, 400 μm optical fiber (1 mm fiber length, ThorLabs) was chronically implanted in the nasal cavity for optogenetic stimulations. Mice were stimulated in their home cage using a 473 nm laser (SLOC Lasers, BL473T8-150FC) coupled to an articulated rotary joint patch cable (ThorLabs). For most experiments, stimulations were comprised of five 150-ms pulses at 0.5 Hz delivered through a protocol written in LabView (National Instruments). When testing the effects of stimulation length, five pulses of length 5, 50, and 150 ms were used. If not otherwise stated, laser stimulation was at the highest intensity that the mouse consistently slept through (ranging from 5 to 30 mW/mm^2). On the first recording day, the stimulus was titrated for each mouse. If the mouse repeatedly woke up to a stimulus intensity (i.e., more than three times), the laser power was lowered. If the mouse did not wake up to multiple stimulations at that intensity, the laser power was increased. Laser intensity was measured at the output from the patch cable using a power meter (ThorLabs) and ranged from 0.7 to 30 mW/mm^2.

Data acquisition—*In vivo* electrophysiological recordings were made by connecting the EIB interface board to an Intan RHD2000 amplifier board (Intan Technologies). Mice were briefly anesthetized with isoflurane then connected to the system. They were given one hour to adapt and recover from anesthesia then recorded for 3–4 hours in their home cages each day (for up to one week) to ensure many state transitions. For mice used for single-unit recordings, after each recording day, a one-third turn of the screw was performed to advance the electrodes ~150 μm (Anikeeva et al., 2011). Signals from each electrode were amplified, filtered between 0.1 Hz to 9 kHz, digitized at 25 kHz, and stored for offline analysis via the RHD data acquisition GUI.

Respiratory recordings were amplified through DP-301 single-channel differential amplifier (Warner Instruments) and filtered from 0.1 Hz to 100 Hz. EEG and EMG recordings were pre-amplified through a four-channel mouse preamplifier (Pinnacle Technology Inc) prior to amplification through DP-304 differential amplifier (Warner Instruments). EMG was filtered between 1 Hz and 30 Hz, and EEG was filtered between 0.1 Hz and 100 Hz. Respiration, EEG, and EMG were simultaneously acquired at 1017 Hz with a RZ5P processor (Tucker-Davis Technologies).

Histology—Mice were deeply anesthetized by intraperitoneal injection of ketamine/ xylazine (200 mg/20 mg per kg body weight) before they were transcardially perfused with PBS and 4% paraformaldehyde. Brains were dissected and additionally fixed overnight in PFA. After fixation, 100 μm coronal vibratome sections were cut, mounted, and stained with Cresyl violet to confirm recording sites. Electrode placement was confirmed for all APC unit recording mice. Placement for LFP recordings was confirmed in a subset of animals and for subsequent animals the presence of responses was used. Figures used the region outlines from the Allen Mouse Brain Common Coordinate Framework version 3 (https:// scalablebrainatlas.incf.org/mouse/ABA_v3) (Lein et al., 2007).

QUANTIFICATION AND STATISTICAL ANALYSIS

Data analysis—Acquired data were processed offline using custom MATLAB (MathWorks) scripts and the Chronux tool box (http://chronux.org/). Brain states were defined based on the LFP and EMG signals (Veasey et al., 2000). Spectrograms of the 0–15 Hz range were calculated using the multitaper methods in the Chronux tool box (MATLAB function: mtspecgramc with a moving window of 0.5 s) (Figure S1A). Trials were excluded if a mouse changed states during a stimulation. Differential LFPs were calculated as the difference between pairs of neighboring electrodes in the same brain area to achieve spatially local measurements of electrical activity and filtered with a bandpass filter of 1–100 Hz. Evoked responses were defined as being two standard deviations above the average LFP amplitude, which was calculated from the whole recording session. Responses to stimulations were extracted and the amplitude was quantified from peak to trough for each stimulation and averaged across trials within each state. To analyze across multiple mice, the LFP amplitude was normalized to that during NREM sleep in each animal (Figures 1, 2, and 5). Additional LFP measures that were analyzed included the area under the curve (MATLAB function: trapz of the absolute value of the LFP) and root-mean-square amplitude (MATLAB function: RMS) of the entire 150-ms stimulation period (Figures S1F and S1G). Gamma oscillations (30–100 Hz) were calculated in 150 ms time segments (MATLAB function: bandpower) and either normalized to the pre-stimulation value in each state (–150 ms) or the pre-stimulation value of NREM sleep (Figure 3). Spectrograms of the gamma range (30–100 Hz) were calculated using the multitaper methods in the Chronux tool box (MATLAB function: mtspecgramc with a moving window of 0.15 s). For spontaneous gamma oscillations, the gamma power was calculated from 1 minute of data in each state and normalized to the total power in the signal. Coherence was calculated in 150 ms time windows: the 150 ms before the stimulus, the 150 ms during the stimulus, and 150 ms after the end of the stimulus. Changes were calculated: PRE-STIM and POST-STIM (Figure 4). The coherence in the gamma band was calculated by averaging the coherence calculated between 33–100 Hz for each mouse. The different gamma range is due to being calculated in 150 ms increments, which led to a resolution of 6.6 Hz. Spontaneous coherence was calculated from 1 minute of activity in each state for each animal.

For single-unit analysis, signals were filtered from 300–5000 Hz. Single units were isolated using the MATLAB wave_clus GUI (Quiroga et al., 2004). Single units had less than 2% of spikes during the 2 ms refractory period. Firing of single units were further analyzed in MATLAB. Spontaneous firing rates were calculated from six 10-second data segments. For evoked responses, spikes were binned in 50 ms increments and converted into Hz. For each laser pulse, the firing rate in each trial was calculated from the 150 ms prior to the stimulation and the 150 ms during the stimulation (Figure 6).

For respiration analysis, multiple 30-second time bins of breathing in each state were analyzed such that each state was equally represented within each animal. For pressure sensor recordings, respiration was analyzed using the BreathMetrics (Noto et al., 2018) package in MATLAB with baseline correction and z-scoring. For thermocouple recordings, amplitude was calculated using the Hilbert transform then z-scored. The power in the

respiratory signal was calculated in 0.5 Hz increments between 0–12 Hz and normalized to the total power in the signal.

Statistical analysis—Statistical analysis was performed in GraphPad Prism 8 (San Diego, CA). Significance was set at $p < 0.05$. In general, the mean ± SEM is shown and reported in figures. Specific statistical tests are referenced in each figure legend. For each mouse in which multiple stimulations were performed, an unpaired t-test was used to determine significance between the states. For normalized population data, Wilcoxon matched-pairs signed rank tests were used for comparisons within the same region in two brain states and Kruskal-Wallis tests for three states. One-way repeated measures ANOVAs followed by Tukey's multiple comparisons tests were used when comparing three states for most non-normalized data. When comparing states across time, two-way repeated measures ANOVAs followed by Sidak's multiple comparisons tests were used.

Supplementary Material

Refer to Web version on PubMed Central for supplementary material.

ACKNOWLEDGMENTS

REFERENCES

Anikeeva P, Andalman AS, Witten I, Warden M, Goshen I, Grosenick L, Gunaydin LA, Frank LM, and Deisseroth K (2011). Optetrode: a multi-channel readout for optogenetic control in freely moving mice. Nat. Neurosci. 15, 163–170. 10.1038/nn.2992. [PubMed: 22138641]

Arzi A, Holtzman Y, Samnon P, Eshel N, Harel E, and Sobel N (2014). Olfactory aversive conditioning during sleep reduces cigarette-smoking behavior. J. Neurosci. 34, 15382–15393. 10.1523/JNEUROSCI.2291-14.2014. [PubMed: 25392505]

Arzi A, Sela L, Green A, Givaty G, Dagan Y, and Sobel N (2010). The influence of odorants on respiratory patterns in sleep. Chem. Senses 35, 31–40. 10.1093/chemse/bjp079. [PubMed: 19917590]

Arzi A, Shedlesky L, Ben-Shaul M, Nasser K, Oksenberg A, Hairston IS, and Sobel N (2012). Humans can learn new information during sleep. Nat. Neurosci. 15, 1460–1465. 10.1038/nn.3193. [PubMed: 22922782]

Badia P, Wesensten N, Lammers W, Culpepper J, and Harsh J (1990). Responsiveness to olfactory stimuli presented in sleep. Physiol. Behav. 48, 87–90. 10.1016/0031-9384(90)90266-7. [PubMed: 2236283]

Barnes DC, Chapuis J, Chaudhury D, and Wilson DA (2011). Odor fear conditioning modifies piriform cortex local field potentials both during conditioning and during post-conditioning sleep. PLoS One 6, e18130. 10.1371/journal.pone.0018130. [PubMed: 21448432]

Barnes DC, and Wilson DA (2014). Slow-wave sleep-imposed replay modulates both strength and precision of memory. J. Neurosci. 34, 5134–5142. 10.1523/JNEUROSCI.5274-13.2014. [PubMed: 24719093]

Bastos AM, Vezoli J, and Fries P (2015). Communication through coherence with inter-areal delays. Curr. Opin. Neurobiol. 31, 173–180. 10.1016/j.conb.2014.11.001. [PubMed: 25460074]

Bhattarai JP, Schreck M, Moberly AH, Luo W, and Ma M (2020). Aversive learning increases release probability of olfactory sensory neurons. Curr. Biol. 30, 31–41.e3. 10.1016/j.cub.2019.11.006. [PubMed: 31839448]

Bolding KA, and Franks KM (2018). Recurrent cortical circuits implement concentration-invariant odor coding. Science 361. 10.1126/science.aat6904.

Boyd AM, Kato HK, Komiyama T, and Isaacson JS (2015). Broadcasting of cortical activity to the olfactory bulb. Cell Rep. 10, 1032–1039. 10.1016/j.celrep.2015.01.047. [PubMed: 25704808]

Boyd AM, Sturgill JF, Poo C, and Isaacson JS (2012). Cortical feedback control of olfactory bulb circuits. Neuron 76, 1161–1174. 10.1016/j.neuron.2012.10.020. [PubMed: 23259951]

Brugge JF, and Merzenich MM (1973). Responses of neurons in auditory cortex of the macaque monkey to monaural and binaural stimulation. J. Neurophysiol. 36, 1138–1158. 10.1152/jn.1973.36.6.1138. [PubMed: 4761724]

Buzsaki G, Anastassiou CA, and Koch C (2012). The origin of extracellular fields and currents–EEG, ECoG, LFP and spikes. Nat. Rev. Neurosci. 13, 407–420. 10.1038/nrn3241. [PubMed: 22595786]

Carskadon MA, and Herz RS (2004). Minimal olfactory perception during sleep: why odor alarms will not work for humans. Sleep 27, 402–405. [PubMed: 15164891]

Chong E, Moroni M, Wilson C, Shoham S, Panzeri S, and Rinberg D (2020). Manipulating synthetic optogenetic odors reveals the coding logic of olfactory perception. Science 368. 10.1126/science.aba2357.

Courtiol E, Hegoburu C, Litaudon P, Garcia S, Fourcaud-Trocme N, and Buonviso N (2011). Individual and synergistic effects of sniffing frequency and flow rate on olfactory bulb activity. J. Neurophysiol. 106, 2813–2824. 10.1152/jn.00672.2011. [PubMed: 21900510]

Courtiol E, and Wilson DA (2014). Thalamic olfaction: characterizing odor processing in the mediodorsal thalamus of the rat. J. Neurophysiol. 111, 1274–1285. 10.1152/jn.00741.2013. [PubMed: 24353302]

Courtiol E, and Wilson DA (2016). The olfactory mosaic: bringing an olfactory network together for odor perception. Perception 46. 10.1177/0301006616663216.

Douglas NJ, White DP, Pickett CK, Weil JV, and Zwillich CW (1982). Respiration during sleep in normal man. Thorax 37, 840–844. 10.1136/thx.37.11.840. [PubMed: 7164002]

Ferezou I, Bolea S, and Petersen CC (2006). Visualizing the cortical representation of whisker touch: voltage-sensitive dye imaging in freely moving mice. Neuron 50, 617–629. 10.1016/j.neuron.2006.03.043. [PubMed: 16701211]

Fontanini A, and Bower JM (2005). Variable coupling between olfactory system activity and respiration in ketamine/xylazine anesthetized rats. J. Neurophysiol. 93, 3573–3581. 10.1152/jn.01320.2004. [PubMed: 15689385]

French AS, Geissmann Q, Beckwith EJ, and Gilestro GF (2021). Sensory processing during sleep in Drosophila melanogaster. Nature 598, 479–482. 10.1038/s41586-021-03954-w. [PubMed: 34588694]

Friedman L, Haines A, Klann K, Gallaugher L, Salibra L, Han F, and Strohl KP (2004). Ventilatory behavior during sleep among A/J and C57BL/6J mouse strains. J. Appl. Physiol. (1985) 97, 1787–1795. 10.1152/japplphysiol.01394.2003. [PubMed: 15475556]

Fries P (2015). Rhythms for cognition: communication through coherence. Neuron 88, 220–235. 10.1016/j.neuron.2015.09.034. [PubMed: 26447583]

Gelbard-Sagiv H, Magidov E, Sharon H, Hendler T, and Nir Y (2018). Noradrenaline modulates visual perception and late visually evoked activity. Curr. Biol. 28, 2239–2249.e36. 10.1016/j.cub.2018.05.051. [PubMed: 29983318]

Gray CM, and Singer W (1989). Stimulus-specific neuronal oscillations in orientation columns of cat visual cortex. Proc. Natl. Acad. Sci. U S A. 86, 1698–1702. [PubMed: 2922407]

Gucer G (1979). Effect of sleep upon the transmission of afferent activity in the somatic afferent system. Exp. Brain Res. 34, 287–298. [PubMed: 217703]

Hauner KK, Howard JD, Zelano C, and Gottfried JA (2013). Stimulus-specific enhancement of fear extinction during slow-wave sleep. Nat. Neurosci. 16, 1553–1555. 10.1038/nn.3527. [PubMed: 24056700]

Hayat H, Regev N, Matosevich N, Sales A, Paredes-Rodriguez E, Krom AJ, Bergman L, Li Y, Lavigne M, Kremer EJ, et al. (2020). Locus coeruleus norepinephrine activity mediates sensory-evoked awakenings from sleep. Sci. Adv. 6, eaaz4232. 10.1126/sciadv.aaz4232. [PubMed: 32285002]

Illig KR, and Haberly LB (2003). Odor-evoked activity is spatially distributed in piriform cortex. J. Comp. Neurol. 457, 361–373. 10.1002/cne.10557. [PubMed: 12561076]

Issa EB, and Wang X (2008). Sensory responses during sleep in primate primary and secondary auditory cortex. J. Neurosci. 28, 14467–14480. 10.1523/JNEUROSCI.3086-08.2008. [PubMed: 19118181]

Issa EB, and Wang X (2011). Altered neural responses to sounds in primate primary auditory cortex during slow-wave sleep. J. Neurosci. 31, 2965–2973. 10.1523/JNEUROSCI.4920-10.2011. [PubMed: 21414918]

Jessberger J, Zhong W, Brankack J, and Draguhn A (2016). Olfactory bulb field potentials and respiration in sleep-wake states of mice. Neural Plast. 2016, 4570831. 10.1155/2016/4570831. [PubMed: 27247803]

Jordan R, Fukunaga I, Kollo M, and Schaefer AT (2018). Active sampling state dynamically enhances olfactory bulb odor representation. Neuron 98, 1214–1228.e15. 10.1016/j.neuron.2018.05.016. [PubMed: 29861286]

Kato HK, Chu MW, Isaacson JS, and Komiyama T (2012). Dynamic sensory representations in the olfactory bulb: modulation by wakefulness and experience. Neuron 76, 962–975. 10.1016/j.neuron.2012.09.037. [PubMed: 23217744]

Kollo M, Schmaltz A, Abdelhamid M, Fukunaga I, and Schaefer AT (2014). Silent' mitral cells dominate odor responses in the olfactory bulb of awake mice. Nat. Neurosci. 17, 1313–1315. 10.1038/nn.3768. [PubMed: 25064849]

Lee SH, and Dan Y (2012). Neuromodulation of brain states. Neuron 76, 209–222. 10.1016/j.neuron.2012.09.012. [PubMed: 23040816]

Lein ES, Hawrylycz MJ, Ao N, Ayres M, Bensinger A, Bernard A, Boe AF, Boguski MS, Brockway KS, Byrnes EJ, et al. (2007). Genome-wide atlas of gene expression in the adult mouse brain. Nature 445, 168–176. 10.1038/nature05453. [PubMed: 17151600]

Lepousez G, and Lledo PM (2013). Odor discrimination requires proper olfactory fast oscillations in awake mice. Neuron 80, 1010–1024. 10.1016/j.neuron.2013.07.025. [PubMed: 24139818]

Li A, Gire DH, Bozza T, and Restrepo D (2014). Precise detection of direct glomerular input duration by the olfactory bulb. J. Neurosci. 34, 16058–16064. 10.1523/JNEUROSCI.3382-14.2014. [PubMed: 25429146]

Li J, Ishii T, Feinstein P, and Mombaerts P (2004). Odorant receptor gene choice is reset by nuclear transfer from mouse olfactory sensory neurons. Nature 428, 393–399. 10.1038/nature02433. [PubMed: 15042081]

Li W, Lopez L, Osher J, Howard JD, Parrish TB, and Gottfried JA (2010). Right orbitofrontal cortex mediates conscious olfactory perception. Psychol. Sci. 21, 1454–1463. 10.1177/0956797610382121. [PubMed: 20817780]

Livingstone MS, and Hubel DH (1981). Effects of sleep and arousal on the processing of visual information in the cat. Nature 291, 554–561. [PubMed: 6165893]

Lorincz ML, and Adamantidis AR (2017). Monoaminergic control of brain states and sensory processing: existing knowledge and recent insights obtained with optogenetics. Prog. Neurobiol. 151, 237–253. 10.1016/j.pneurobio.2016.09.003. [PubMed: 27634227]

Madisen L, Mao T, Koch H, Zhuo JM, Berenyi A, Fujisawa S, Hsu YW, Garcia AJ 3rd, Gu X, Zanella S, et al. (2012). A toolbox of Cre-dependent optogenetic transgenic mice for light-induced activation and silencing. Nat. Neurosci. 15, 793–802. 10.1038/nn.3078. [PubMed: 22446880]

Mainland J, and Sobel N (2006). The sniff is part of the olfactory percept. Chem. Senses 31, 181–196. 10.1093/chemse/bjj012. [PubMed: 16339268]

McCormick DA, McGinley MJ, and Salkoff DB (2015). Brain state dependent activity in the cortex and thalamus. Curr. Opin. Neurobiol. 31, 133–140. 10.1016/j.conb.2014.10.003. [PubMed: 25460069]

Miura K, Mainen ZF, and Uchida N (2012). Odor representations in olfactory cortex: distributed rate coding and decorrelated population activity. Neuron 74, 1087–1098. 10.1016/j.neuron.2012.04.021. [PubMed: 22726838]

Mori K, Manabe H, Narikiyo K, and Onisawa N (2013). Olfactory consciousness and gamma oscillation couplings across the olfactory bulb, olfactory cortex, and orbitofrontal cortex. Front. Psychol. 4, 743. 10.3389/fpsyg.2013.00743. [PubMed: 24137148]

Mori K, and Sakano H (2011). How is the olfactory map formed and interpreted in the mammalian brain? Annu. Rev. Neurosci. 34, 467–499. 10.1146/annurev-neuro-112210-112917. [PubMed: 21469960]

Mori K, and Sakano H (2021). Olfactory circuitry and behavioral decisions. Annu. Rev. Physiol. 83, 231–256. 10.1146/annurev-physiol-031820-092824. [PubMed: 33228453]

Murakami M, Kashiwadani H, Kirino Y, and Mori K (2005). State-dependent sensory gating in olfactory cortex. Neuron 46, 285–296. 10.1016/j.neuron.2005.02.025. [PubMed: 15848806]

Murata K, and Kameda K (1963). The activity of single cortical neurones of unrestrained cats during sleep and wakefulness. Arch. Ital. Biol. 101, 306–331. [PubMed: 14166963]

Nir Y, Vyazovskiy VV, Cirelli C, Banks MI, and Tononi G (2015). Auditory responses and stimulus-specific adaptation in rat auditory cortex are preserved across NREM and REM sleep. Cereb. Cortex 25, 1362–1378. 10.1093/cercor/bht328. [PubMed: 24323498]

Noto T, Zhou G, Schuele S, Templer J, and Zelano C (2018). Automated analysis of breathing waveforms using BreathMetrics: a respiratory signal processing toolbox. Chem. Senses 43, 583–597. 10.1093/chemse/bjy045. [PubMed: 29985980]

Otazu GH, Chae H, Davis MB, and Albeanu DF (2015). Cortical feedback decorrelates olfactory bulb output in awake mice. Neuron 86, 1461–1477. 10.1016/j.neuron.2015.05.023. [PubMed: 26051422]

Pereira A, Ribeiro S, Wiest M, Moore LC, Pantoja J, Lin SC, and Nicolelis MA (2007). Processing of tactile information by the hippocampus. Proc. Natl. Acad. Sci. U S A. 104, 18286–18291. 10.1073/pnas.0708611104. [PubMed: 17989221]

Plailly J, Howard JD, Gitelman DR, and Gottfried JA (2008). Attention to odor modulates thalamocortical connectivity in the human brain. J. Neurosci. 28, 5257–5267. 10.1523/JNEUROSCI.5607-07.2008. [PubMed: 18480282]

Poo C, and Isaacson JS (2009). Odor representations in olfactory cortex: "sparse" coding, global inhibition, and oscillations. Neuron 62, 850–861. 10.1016/j.neuron.2009.05.022. [PubMed: 19555653]

Price JL, and Slotnick BM (1983). Dual olfactory representation in the rat thalamus: an anatomical and electrophysiological study. J. Comp. Neurol. 215, 63–77. 10.1002/cne.902150106. [PubMed: 6853766]

Qiu Q, Wu Y, Ma L, and Yu CR (2021). Encoding innately recognized odors via a generalized population code. Curr. Biol. 31, 1813–1825.e14. 10.1016/j.cub.2021.01.094. [PubMed: 33651991]

Quiroga RQ, Nadasdy Z, and Ben-Shaul Y (2004). Unsupervised spike detection and sorting with wavelets and superparamagnetic clustering. Neural Comput. 16, 1661–1687. 10.1162/089976604774201631. [PubMed: 15228749]

Rasch B, Buchel C, Gais S, and Born J (2007). Odor cues during slow-wave sleep prompt declarative memory consolidation. Science 315, 1426–1429. 10.1126/science.1138581. [PubMed: 17347444]

Rebello MR, McTavish TS, Willhite DC, Short SM, Shepherd GM, and Verhagen JV (2014). Perception of odors linked to precise timing in the olfactory system. PLoS Biol. 12, e1002021. 10.1371/journal.pbio.1002021. [PubMed: 25514030]

Redinbaugh MJ, Phillips JM, Kambi NA, Mohanta S, Andryk S, Dooley GL, Afrasiabi M, Raz A, and Saalmann YB (2020). Thalamus modulates consciousness via layer-specific control of cortex. Neuron 106, 66–75.e12. 10.1016/j.neuron.2020.01.005. [PubMed: 32053769]

Rennaker RL, Chen CF, Ruyle AM, Sloan AM, and Wilson DA (2007). Spatial and temporal distribution of odorant-evoked activity in the piriform cortex. J. Neurosci. 27, 1534–1542. 10.1523/JNEUROSCI.4072-06.2007. [PubMed: 17301162]

Rinberg D, Koulakov A, and Gelperin A (2006). Sparse odor coding in awake behaving mice. J. Neurosci. 26, 8857–8865. 10.1523/JNEUROSCI.0884-06.2006. [PubMed: 16928875]

Rolls A, Makam M, Kroeger D, Colas D, de Lecea L, and Heller HC (2013). Sleep to forget: interference of fear memories during sleep. Mol. Psychiatry 18, 1166–1170. 10.1038/mp.2013.121. [PubMed: 24081009]

Sela Y, Vyazovskiy VV, Cirelli C, Tononi G, and Nir Y (2016). Responses in rat core auditory cortex are preserved during sleep spindle oscillations. Sleep 39, 1069–1082. 10.5665/sleep.5758. [PubMed: 26856904]

Shanahan LK, Gjorgieva E, Paller KA, Kahnt T, and Gottfried JA (2018). Odor-evoked category reactivation in human ventromedial prefrontal cortex during sleep promotes memory consolidation. Elife 7. 10.7554/eLife.39681.

Sharon O, and Nir Y (2018). Attenuated fast steady-state visual evoked potentials during human sleep. Cereb. Cortex 28, 1297–1311. 10.1093/cercor/bhx043. [PubMed: 28334175]

Singer W, and Gray CM (1995). Visual feature integration and the temporal correlation hypothesis. Annu. Rev. Neurosci. 18, 555–586. 10.1146/annurev.ne.18.030195.003011. [PubMed: 7605074]

Smear M, Resulaj A, Zhang J, Bozza T, and Rinberg D (2013). Multiple perceptible signals from a single olfactory glomerulus. Nat. Neurosci. 16, 1687–1691. 10.1038/nn.3519. [PubMed: 24056698]

Smear M, Shusterman R, O'Connor R, Bozza T, and Rinberg D (2011). Perception of sniff phase in mouse olfaction. Nature 479, 397–400. 10.1038/nature10521. [PubMed: 21993623]

Stern M, Bolding KA, Abbott LF, and Franks KM (2018). A transformation from temporal to ensemble coding in a model of piriform cortex. Elife 7. 10.7554/eLife.34831.

Stettler DD, and Axel R (2009). Representations of odor in the piriform cortex. Neuron 63, 854–864. 10.1016/j.neuron.2009.09.005. [PubMed: 19778513]

Stopfer M, Bhagavan S, Smith BH, and Laurent G (1997). Impaired odour discrimination on desynchronization of odour-encoding neural assemblies. Nature 390, 70–74. 10.1038/36335. [PubMed: 9363891]

Stuck BA, Stieber K, Frey S, Freiburg C, Hormann K, Maurer JT, and Hummel T (2007). Arousal responses to olfactory or trigeminal stimulation during sleep. Sleep 30, 506–510. 10.1093/sleep/30.4.506. [PubMed: 17520795]

Stuck BA, Weitz H, Hormann K, Maurer JT, and Hummel T (2006). Chemosensory event-related potentials during sleep–a pilot study. Neurosci. Lett. 406, 222–226. 10.1016/j.neulet.2006.07.068. [PubMed: 16934401]

Tham WW, Stevenson RJ, and Miller LA (2011). The role of the mediodorsal thalamic nucleus in human olfaction. Neurocase 17, 148–159. 10.1080/13554794.2010.504728. [PubMed: 20818539]

Veasey SC, Valladares O, Fenik P, Kapfhamer D, Sanford L, Benington J, and Bucan M (2000). An automated system for recording and analysis of sleep in mice. Sleep 23, 1025–1040. [PubMed: 11145318]

Verhagen JV, Wesson DW, Netoff TI, White JA, and Wachowiak M (2007). Sniffing controls an adaptive filter of sensory input to the olfactory bulb. Nat. Neurosci. 10, 631–639. 10.1038/nn1892. [PubMed: 17450136]

Vesuna S, Kauvar IV, Richman E, Gore F, Oskotsky T, Sava-Segal C, Luo L, Malenka RC, Henderson JM, Nuyujukian P, et al. (2020). Deep posteromedial cortical rhythm in dissociation. Nature 586, 87–94. 10.1038/s41586-020-2731-9. [PubMed: 32939091]

Vetere G, Tran LM, Moberg S, Steadman PE, Restivo L, Morrison FG, Ressler KJ, Josselyn SA, and Frankland PW (2019). Memory formation in the absence of experience. Nat. Neurosci. 22, 933–940. 10.1038/s41593-019-0389-0. [PubMed: 31036944]

Vincis R, Gschwend O, Bhaukaurally K, Beroud J, and Carleton A (2012). Dense representation of natural odorants in the mouse olfactory bulb. Nat. Neurosci. 15, 537–539. 10.1038/nn.3057. [PubMed: 22406552]

Wachowiak M (2011). All in a sniff: olfaction as a model for active sensing. Neuron 71, 962–973. 10.1016/j.neuron.2011.08.030. [PubMed: 21943596]

Wachowiak M, Economo MN, Diaz-Quesada M, Brunert D, Wesson DW, White JA, and Rothermel M (2013). Optical dissection of odor information processing in vivo using GCaMPs expressed in specified cell types of the olfactory bulb. J. Neurosci. 33, 5285–5300. 10.1523/JNEUROSCI.4824-12.2013. [PubMed: 23516293]

Weber F, Chung S, Beier KT, Xu M, Luo L, and Dan Y (2015). Control of REM sleep by ventral medulla GABAergic neurons. Nature 526, 435–438. 10.1038/nature14979. [PubMed: 26444238]

Wesson DW, Donahou TN, Johnson MO, and Wachowiak M (2008). Sniffing behavior of mice during performance in odor-guided tasks. Chem. Senses 33, 581–596. 10.1093/chemse/bjn029. [PubMed: 18534995]

Wesson DW, Verhagen JV, and Wachowiak M (2009). Why sniff fast? The relationship between sniff frequency, odor discrimination, and receptor neuron activation in the rat. J. Neurophysiol. 101, 1089–1102. 10.1152/jn.90981.2008. [PubMed: 19052108]

Wilson DA (2010). Single-unit activity in piriform cortex during slow-wave state is shaped by recent odor experience. J. Neurosci. 30, 1760–1765. 10.1523/JNEUROSCI.5636-09.2010. [PubMed: 20130185]

Wilson DA, and Yan X (2010). Sleep-like states modulate functional connectivity in the rat olfactory system. J. Neurophysiol. 104, 3231–3239. 10.1152/jn.00711.2010. [PubMed: 20861440]

Yarita H, Iino M, Tanabe T, Kogure S, and Takagi SF (1980). A transthalamic olfactory pathway to orbitofrontal cortex in the monkey. J. Neurophysiol. 43, 69–85. 10.1152/jn.1980.43.1.69. [PubMed: 6766180]

Yuzgec O, Prsa M, Zimmermann R, and Huber D (2018). Pupil size coupling to cortical states protects the stability of deep sleep via parasympathetic modulation. Curr. Biol. 28, 392–400.e93. 10.1016/j.cub.2017.12.049. [PubMed: 29358069]

Highlights

- OSN stimulations evoke larger olfactory LFPs in NREM and REM sleep than in wakefulness

- Larger responses in sleep suggest the lack of a central gate in the olfactory pathway

- More OB and APC units respond in NREM with a higher incidence of suppressed firing

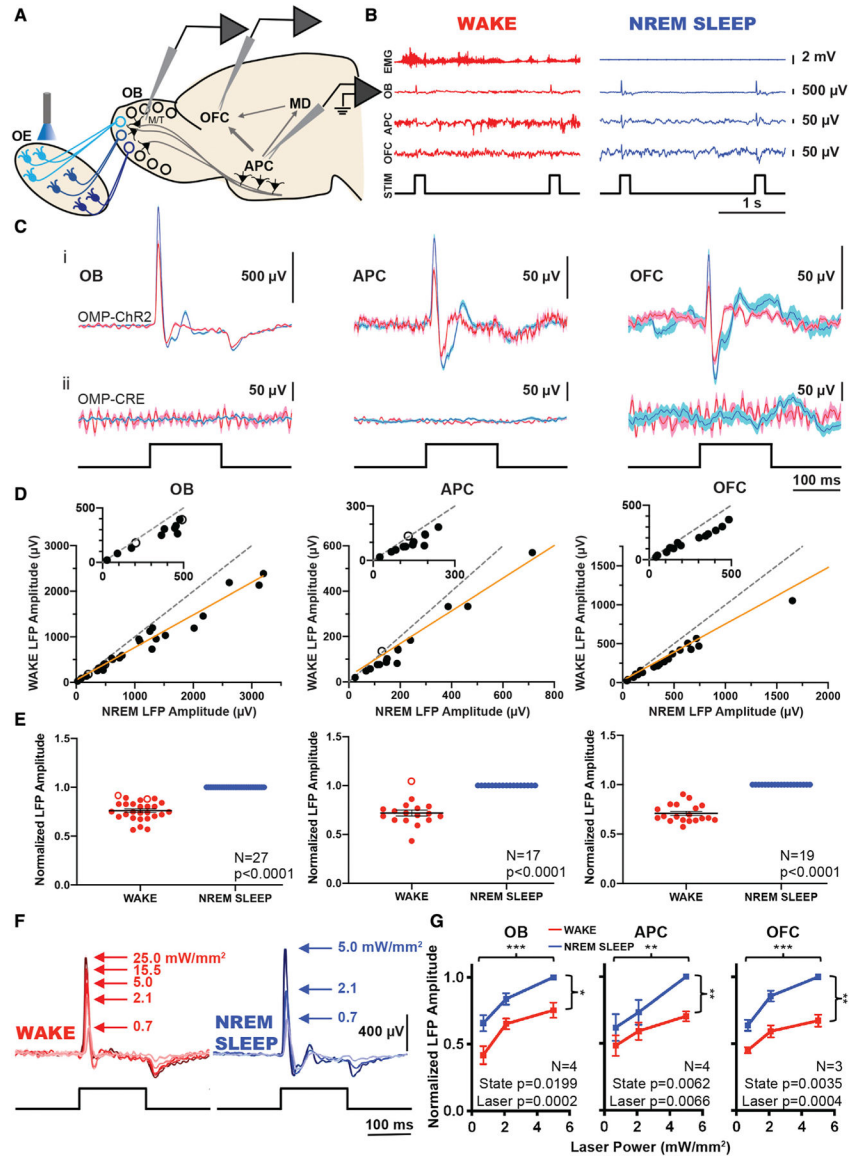- Slower and shallower breathing could partially gate olfactory input in sleep

Figure 1. Optogenetic stimulation of OSNs in the nasal epithelium evokes stronger LFP responses during NREM SLEEP than during WAKE

(A) Schematic of recording setup.

(B) Raw traces from all three regions from a single mouse. WAKE is in red and NREM SLEEP is in blue in all panels.

(C) The average of 20 traces (mean ± SEM) in each state in an OMP-ChR2 mouse (i) and an OMP-CRE control mouse (ii). Note the larger amplitudes of the LFP during NREM SLEEP compared with WAKE in the OMP-ChR2 mouse.

(D) Relationship of the LFP amplitudes under NREM SLEEP versus WAKE in each region. For each animal, an unpaired t test was performed from multiple stimulations in each state, with an average number of trials of around 35. Filled circles indicate a significant difference between the two states, while hollow circles indicate no significant difference. For the APC, one point falls outside the axes (4,464 μV, 2,889 μV). The identity line is in gray (dashed) and the best fit line in orange (solid).

(E) The LFP amplitude (mean ± SEM) was normalized to the NREM SLEEP state for each mouse. OB n = 27 mice (13 males and 14 females), APC n = 17 (12 and 5), and OFC n = 19 (10 and 9). Wilcoxon matched-pairs signed-rank test shows significant differences in all regions.

(F) The average of 20 OB traces (mean ± SEM) at different laser intensities from the same mouse in WAKE and NREM SLEEP states.

(G) For each mouse, the LFP amplitude (mean ± SEM) was normalized to that in the NREM SLEEP at the highest laser intensity (5.0 mW/mm^2). Two-way repeated-measures ANOVAs were performed and both factors (state and laser power) were significantly different in all three regions; *$p < 0.05$, **$p < 0.01$, ***$p < 0.001$, and ****$p < 0.0001$. See also Figure S1.
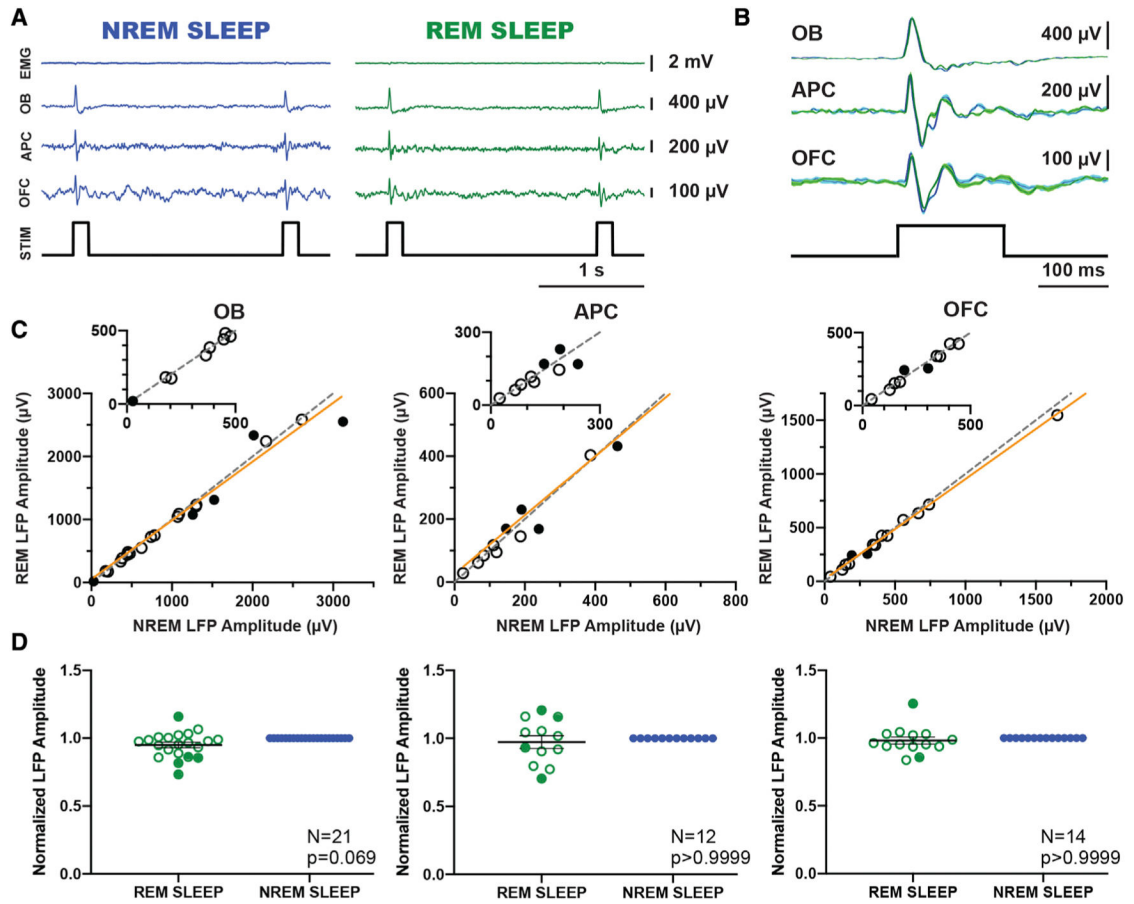
Figure 2. Optogenetic stimulation of OSNs in the nasal epithelium evokes similar LFP responses during NREM and REM SLEEP

(A) Raw traces from all three regions from a single mouse. NREM SLEEP is in blue and REM SLEEP is in green in all panels.

(B) The average of 10 traces (mean ± SEM) in each sleep state in an OMP-ChR2 mouse.

(C) Relationship of the LFP amplitudes during NREM SLEEP versus REM SLEEP in each region. For each animal, an unpaired t test was performed from multiple stimulations in each state, with an average of 35 stimulations in NREM and 10 stimulations in REM. Filled circles indicate a significant difference between the two states, while hollow circles indicate no significant difference. For the APC, one point falls outside the axes (4,464 μV, 4,036 μV). The identity line is in gray (dashed) and the best fit line in orange (solid).

(D) The LFP amplitude (mean ± SEM) was normalized to the NREM SLEEP state for each mouse: OB n = 21 mice (10 males and 11 females), APC n = 12 (9 and 3), and OFC n = 14 (7 and 7). Kruskal-Wallis tests were used to determine significance between all three states. The p values reported are from Dunn's multiple comparisons test between NREM and REM. See also Figure S2.
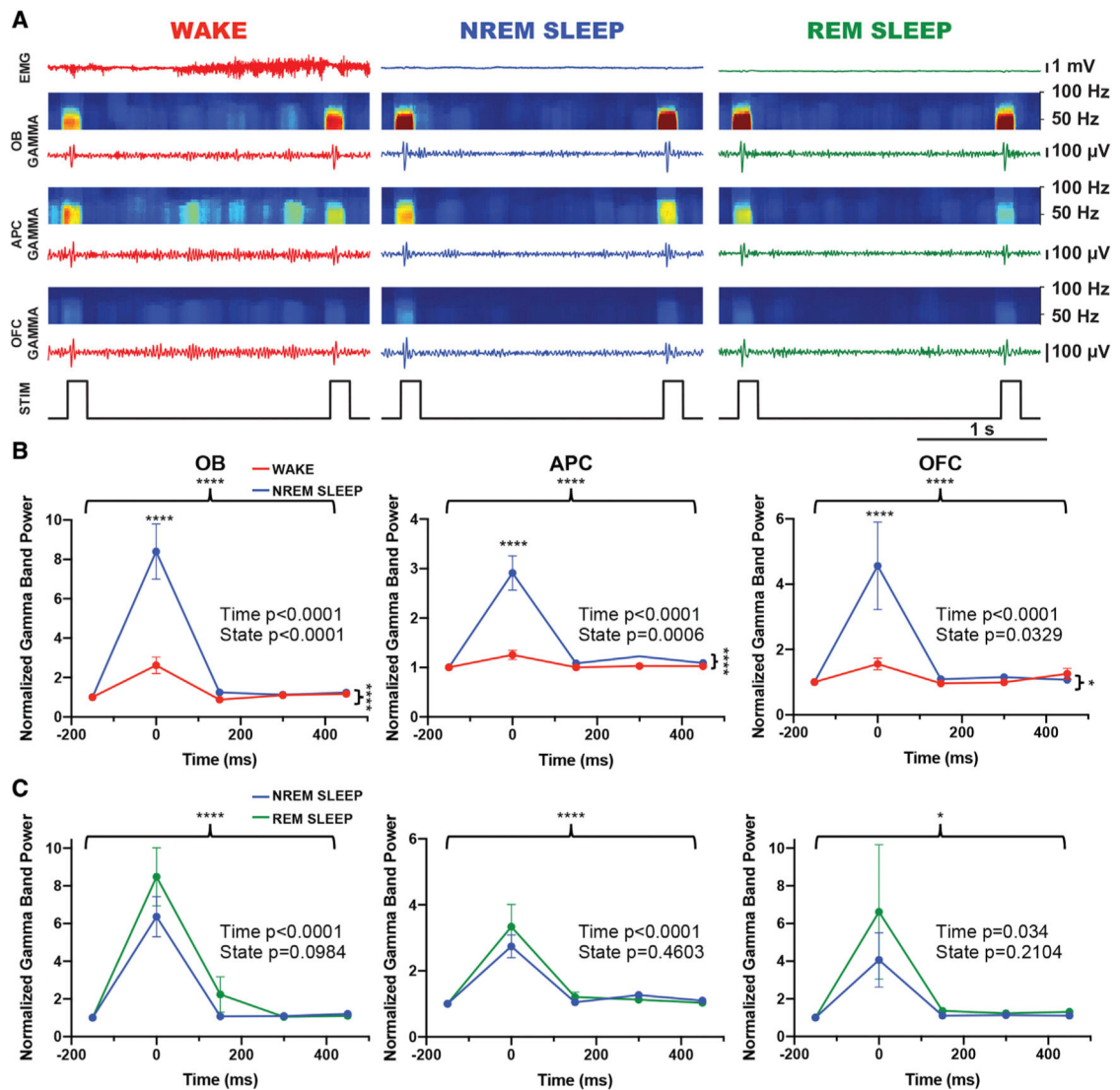
Figure 3. OSN stimulation-induced gamma-band oscillations show greater increases during SLEEP than WAKE

(A) Raw traces of EMG, gamma oscillations (30–100 Hz), power spectra, and stimulation from the same mouse in the OB, APC, and OFC. WAKE is in red, NREM SLEEP is in blue, and REM SLEEP is in green in all panels.

(B) Comparison of gamma oscillations between WAKE and NREM SLEEP normalized to the pre-stimulation value in each state. OB n = 27, APC n = 17, and OFC n = 19 (mean ± SEM). Two-way repeated measures ANOVAs were performed followed by Sidak's multiple comparisons tests.

(C) Comparison of stimulation-induced gamma oscillations between NREM SLEEP and REM SLEEP normalized to the pre-stimulation value in each state. OB n= 21, APC n = 12, and OFC n = 14 (mean ± SEM). The same statistics were used as in (B); *p < 0.05 and ****p < 0.0001. See also Figure S3.
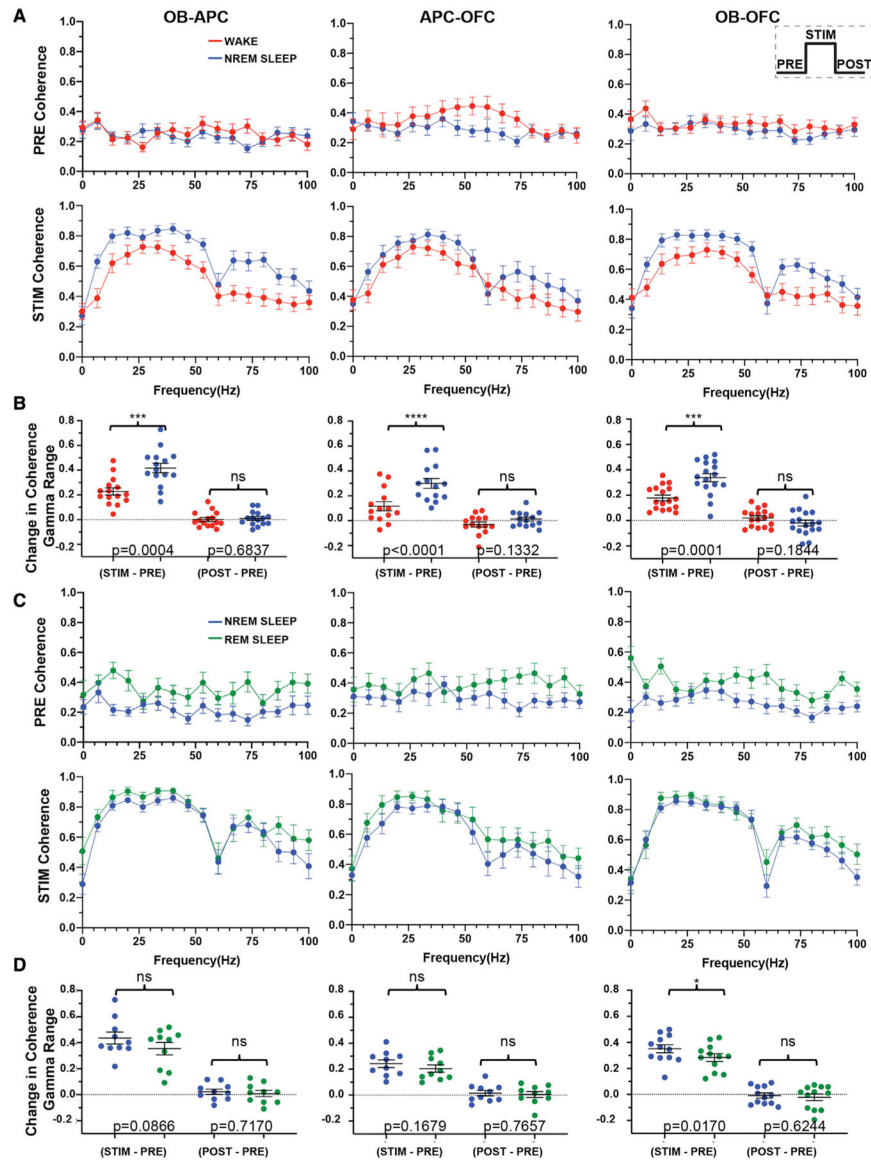
Figure 4. OSN stimulation-induced cross-region coherence shows greater increases in SLEEP than WAKE

(A and B) Comparisons between WAKE and NREM. (A) Coherence during the 150 ms before the stimulation (PRE Coherence) and the 150 ms during the stimulation (STIM Coherence). WAKE is in red and NREM SLEEP is in blue. (B) Changes in gamma-band coherence were calculated as coherence differences from three time periods: STIM-PRE and POST-PRE (see inset in the top right corner of [A]). OB-APC n = 15 (10 males and 5 females), APC-OFC n = 14 (10 and 4), and OB-OFC n = 17 (8 and 9). Significance was determined from paired t tests.

(C and D) Comparisons between NREM and REM. NREM SLEEP is in blue and REM SLEEP is in green. Changes in coherence were calculated as in (B). OB-APC n = 10 (7 and 3), APC-OFC n = 10 (7 and 3), and OB-OFC n = 12 (5 and 7). Data are reported as mean ± SEM. *p < 0.05, ***p < 0.001, and ****p < 0.0001; ns, non-significant. See also Figure S4.
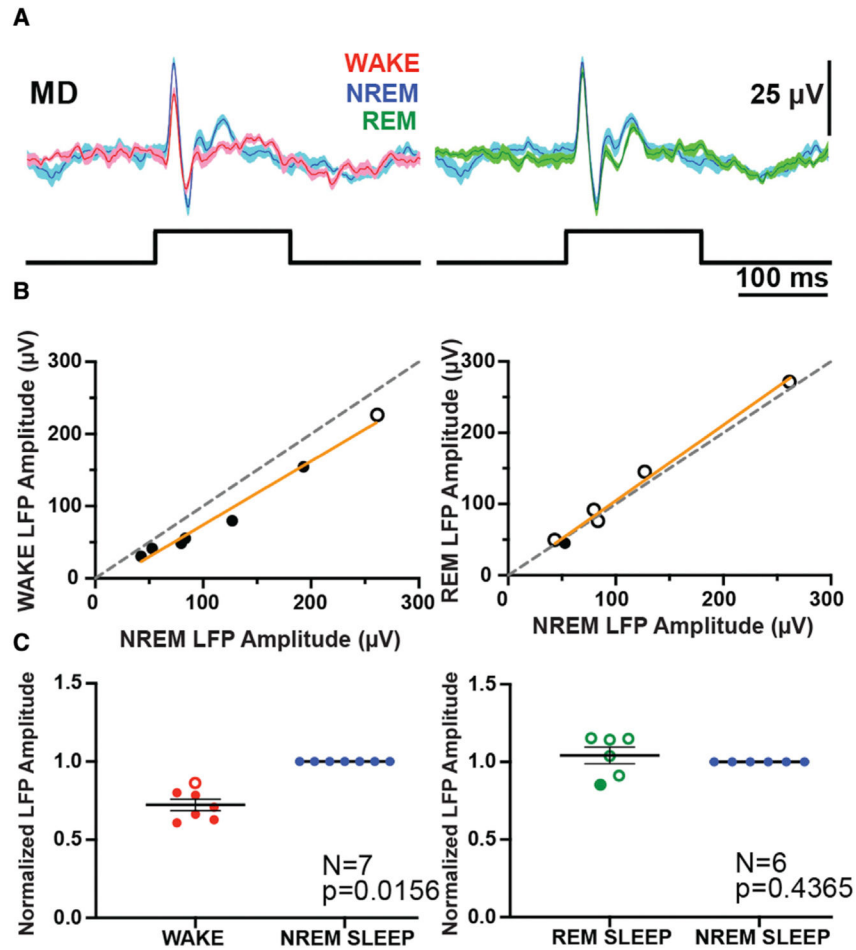
Figure 5. OSN stimulation evokes larger LFP responses during SLEEP than during WAKE in the MD thalamus

(A) The average of 10 traces (mean ± SEM) of WAKE (red), NREM SLEEP (blue), and REM SLEEP (green) from a single mouse.

(B) Cross-state relationship of the LFP amplitudes in individual animals: NREM SLEEP versus WAKE (left) and NREM versus REM SLEEP (right). As in Figure 2, unpaired t tests were performed from multiple stimulations in each state for each animal, with an average of 34 stimulations in WAKE, 33 in NREM, and 6 in REM. Filled circles indicate a significant difference between the two states, while hollow circles indicate no significant difference. The identity line is in gray (dashed) and the best fit line in orange (solid).

(C) The LFP amplitude (mean ± SEM) was normalized for each mouse to the NREM SLEEP state. Wilcoxon matched-pairs signed rank test shows a significant difference between WAKE and NREM SLEEP but not between NREM SLEEP and REM SLEEP. See also Figure S5.
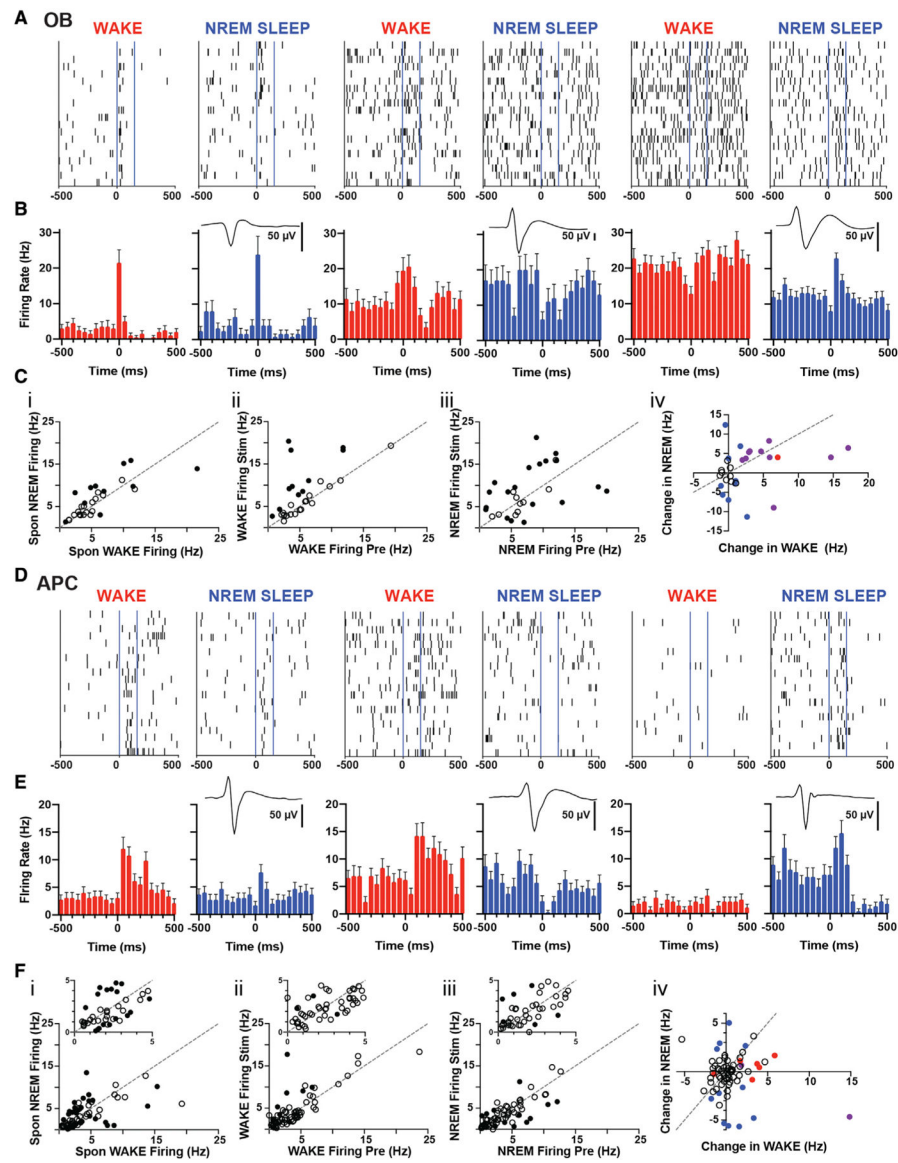
Figure 6. More OB and APC units change firing rates upon OSN stimulation during NREM SLEEP than during WAKE

(A) Raster plots showing 20 trials in each state for three example neurons in OB.

(B) Histograms generated from the average firing rates (mean ± SEM). Insets are average waveforms from 100 spikes of each unit.

(C) Population statistics of 29 OB units (n = 12 mice, 6 males and 6 females). Spontaneous firing rate (i), PRE (150 ms before stimulation) versus STIM (during 150 ms stimulation) firing rates in WAKE (ii), and PRE versus STIM firing rates in NREM (iii) are plotted. Filled circles indicate a significant difference (p < 0.05) between states using unpaired t tests (i) or paired t tests (ii and iii), while hollow circles indicate no significant difference. The dashed gray line is the identity line. Change in firing (iv) was calculated as the firing rate difference between STIM and PRE. Significant changes in WAKE only (red circles), in NREM only (blue), and in both states (purple) and no significant changes (hollow) are shown.

(D–F) Single-unit firing in the APC (68 units from n = 11 mice, 6 males and 5 females). The same calculations were done as in (A–C), respectively. See also Figure S6 and Table S1.
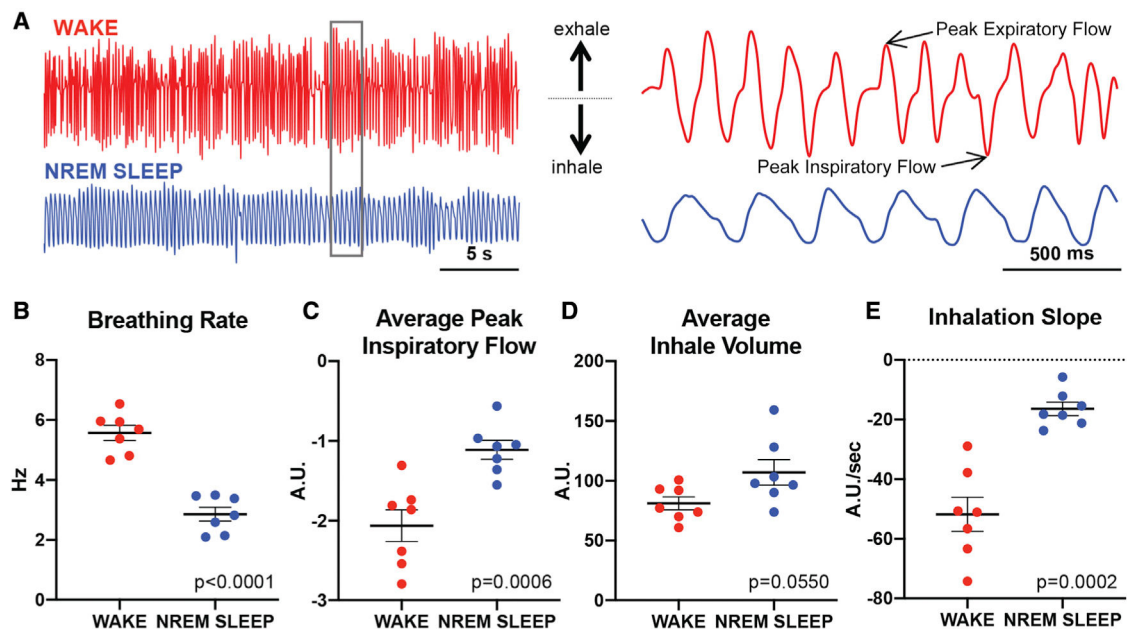
Figure 7. Respiration patterns differ between WAKE and NREM SLEEP

(A) Example 30 s respiration in WAKE and NREM SLEEP from the same mouse. The enlarged 2 s segment depicts various aspects of the signal analyzed. n = 7 mice (3 males and 4 females).

(B–E) Comparison of various respiration parameters between the two states (mean ± SEM): breathing rate (B), average peak inspiratory flow (C), average inhalation volume (D), and inhalation slope (E). Additional parameters are shown in Figure S7A. Multiple 30 s segments (5–8) were used per mouse with an equal number of segments in each state. Paired t tests were used to determine significance. See also Figure S7.

KEY RESOURCES TABLE

REAGENT or RESOURCE	SOURCE	IDENTIFIER
Experimental models: Organisms/strains		
Mouse: OMP-Cre	Jackson Laboratory	RRID:IMSR_JAX:006668
Mouse: Ai32	Jackson Laboratory	RRID:IMSR_JAX:024109
Software and algorithms		
MATLAB	MathWorks	https://www.mathworks.com/products/matlab.html (RRID:SCR_001622)
LabVIEW	National Instruments	https://www.ni.com/en-us/shop/software/products/labview.html (RRID:SCR_014325)
RHX Data Acquisition Software	Intan Technologies	https://intantech.com/RHX_software.html
Chronux Version 2.11	Open-source originally through the Mitra Lab in Cold Spring Harbor	http://chronux.org (RRID:SCR_005547)
Wave_clus	Quiroga et al. (2004)	https://github.com/csn-le/wave_clus (RRID:SCR_016101)
BreathMetrics	Noto et al. (2018)	https://github.com/zelanolab/breathmetrics